Journal of Bionic Engineering (2023) 20:1917–1929
https://doi.org/10.1007/s42235-023-00364-8

RESEARCH ARTICLE

Mechanical Characteristics Analysis of 3D-printing Novel Chiral Honeycomb Array Structures Based on Functional Principle and Constitutive Relationship

Ruiyao Liu[1] · Guofeng Yao[1] · Zezhou Xu[2] · Xue Guo[2] · Jianyong Li[2] · Zhenglei Yu[2,3] · Ping Liang[2] · Zhihui Zhang[2] · Chunyang Han[4]

Received: 21 November 2022 / Revised: 18 February 2023 / Accepted: 21 February 2023 / Published online: 23 March 2023

Abstract
Four novel chiral honeycomb structures inspired by the biological arrangement shape are designed. The functional principle is raised to solve the large deformation of bio-inspired structures and the structural constitutive model is proposed to explain the quasi-static mechanical properties of chiral honeycomb array structures and honeycomb structures. Simulation and experiment results verify the accuracy of theoretical analysis results and the errors are all within 15%. In structural mechanical properties, Equidimensional Chiral Honeycomb Array Structure (ECHS) has excellent mechanical properties. Among ECHS, Small-sized Column Chiral Honeycomb Array Structure (SCHCS) has the best properties. The bearing capacity, specific energy absorption, and specific strength of SCHCS are more than twice as much as the others in this paper. The chiral honeycomb array structure has the best mechanical properties at a certain size. In the structural design, the optimal size model should be obtained first in combination with the optimization algorithm for the protection design.

Keywords Bionic · Gradient sizes · Function principle · Constitutive model · The global simulated annealing optimization algorithm

1 Introduction

In transportation, the violent crash injures passengers [1–3]. To better protect passengers and improve the vehicle protective behaviors, numerous efficient protective structures came into being [4]. More and more protective structures with excellent functional behaviors, which have been widely used in the fields of aerospace [5], transport vehicles protection [6], have been designed. In structural protection applications, bio-inspired structures have outstanding protection features [7]. Among bio-inspired protective structures, honeycomb structure [8], chiral structure [9], and so on have been widely researched. For example, beetle coleopteran could availably defend the beetle from harm. Based on the beetle coleopteran cell consisted of spiral tissue, Zhang et al. [9] imitated the beetle tissue cells to design and manufacture the chiral structures and found that chiral structures with torsional characteristics had excellent bearing and energy-absorbing behaviors. To better study the structural deformation mechanism, Alderson et al. [10] derived Poisson ratio and elastic modulus formula of honeycomb structure by taking honeycomb structures as an example, and explained the structural deformation mechanism. Tobias et al. [11] designed a novel chiral structure based on the compression-torsion coupling effect to achieve stable structural deformation. To further study the compression–torsional characteristics of the bio-inspired chiral structure, Lin et al. [12] accurately predicted the buckling stress of the chiral structure on account of the Cosserat theory. Based on the mechanism that the chiral

✉ Zhenglei Yu
zlyu@jlu.edu.cn

✉ Ping Liang
Liangping@jlu.edu.cn

[1] Department of Mechanics, School of Mechanical and Aerospace Engineering, Jilin University, Changchun 130022, China

[2] Key Laboratory of Bionic Engineering of Ministry of Education, Jilin University, Changchun 130022, China

[3] State Key Laboratory of Automotive Simulation and Control, Jilin University, Changchun 130022, China

[4] Changchun Institute of Optics, Fine Mechanics and Physics, Chinese Academy of Sciences, Changchun 130022, China

inclined bar converts the axial compression load into torsional load, Zhong et al. [13] proposed a novel chiral structure with mechanical properties. In general, the single bio-inspired functional structure could not meet the engineering applications requirements. Therefore, the gradient coupling structure appeared at the right moment, such as the bistable honeycomb structure [14] and the variable gradient honeycomb structure [15]. Combining the steady couple system, David et al. [16] designed the bistable honeycomb structure with excellent energy absorption and recovery properties. Taking regular hexagons with gradient density changes and honeycomb with irregular arrangement as the basic structure, Amin et al. [17] verified its dynamic crushing behaviors in plane. However, there are few comparative studies on the mechanical properties of different types of gradient chiral honeycomb array structures, which were applicable to the crashworthiness field. Therefore, it is chosen to design multiple chiral honeycomb structures in this paper.

In the manufacturing of functional structures, traditional manufacturing processes could not be used for complex structural manufacturing due to the complexity of the bio-inspired structure [18, 19]. However, the emergence of additive manufacturing solved this manufacturing problem [20]. Complex structures with excellent mechanical properties are produced by additive manufacturing [21]. Chang et al. [22] utilized additive manufacturing to manufacture a novel chiral negative Poisson structure, and analyzed structural mechanical properties numerically and experimentally. To study the compression characteristics of honeycomb wing panels in different manufacturing methods, Zhang et al. [23] conducted structural functional tests on bio-inspired structures under different forming methods. Taking the bone cortex of Glyptotherium arizonae as the archetype, Plessis et al. [24] found that the combination of dense layer and porous lattice could provide an optimal energy absorption. Wang et al. [25] made use of additive manufacturing technology to prepare a variety of complex porous structures and compared the properties of prepared structures and manufacturing effects. Obviously, on account of the complexity of modern bio-inspired optimized structures, traditional production methods could no longer meet the production requirements, and the development of additive manufacturing technology simplifies the manufacturing process to a large extent [26]. Moreover, all the research works showed that additive manufacturing of bio-inspired structures had a high credibility. In many scientific researches and practical application structures [27], additive manufacturing technology has been used in the manufacture of complex structures.

In this paper, According to the biological arrangement shape, bio-inspired chiral honeycomb structures are formed: Large Column Honeycomb Chiral Structure (LCHCS), Small Column Honeycomb Chiral Structure (SCHCS), Gradient Honeycomb Chiral Structure (GHCS), and Hourglass Honeycomb Chiral Structure (HHCS), as shown in Fig. 1. The bionic honeycomb structure is used as a reference to compare the excellent characteristics of the novel bionic structures, and the honeycomb structure is arranged and compared in a similar way to improve the reference: Big Honeycomb Structure (BHS), Small Honeycomb Structure (SHS). Due to the complexity of bio-inspired structures, the bio-inspired optimized structures are manufactured by 3D-printing technology. The mechanical characteristics of bio-inspired structures are detected by quasi-static compression experiments and simulations. Functional principle and deformation theory are used to illustrate the mechanical characteristics of the bio-inspired models. Finally, based on the compression force and deformation relationship of the bio-inspired structures, the constitutive model is constructed to further illustrate the compressive bearing characteristics of the bio-inspired structures.

2 Bio-inspired Structures' Experiments and Simulations Analysis

Four kinds of chiral honeycomb structures and two honeycomb structures are considered in this study. The bio-inspired cells consist of the beam. Where, the thickness of the beam is t, $t=1$, $n_x=6$, $n_y=3$, and $n_z=3$ cells in x, y, and z directions are cells. And the gradient difference depends on the size of the top honeycomb and bottom honeycomb. Bio-inspired structures are assembled in this paper by the sequential crossings of front to front, front to back. And then six kinds of cells are combined to obtain six kinds of bio-inspired structures. The mass of six kinds of nylon bio-inspired structures is shown in Table 1.

In this paper, bio-inspired structures are manufactured based on the additive manufacturing machine (FS 403P). Nylon material is selected. At the same time, the performance of samples is easily affected by 3D-printing parameters, which may lead to subtle differences in the material interior. Therefore, material performance tests of printing tensile samples are carried out. The 3D print parameters are shown in Table 2.

When using LS-DYNA for simulation analysis, accurate material property setting can greatly improve the accuracy of simulation analysis. Because #24 material card can be directly input into the material stretching curve for simulation, this study uses #24 material card for simulations and direct import nylon tensile properties curve. The density of nylon material is 1.1×10^{-10} kg/m^3. The Poisson ratio of nylon material is 0.34. The elasticity modulus of nylon material is 1000 MPa. The tensile experiment at room temperature is carried out on DDL100 testing machine. The tensile

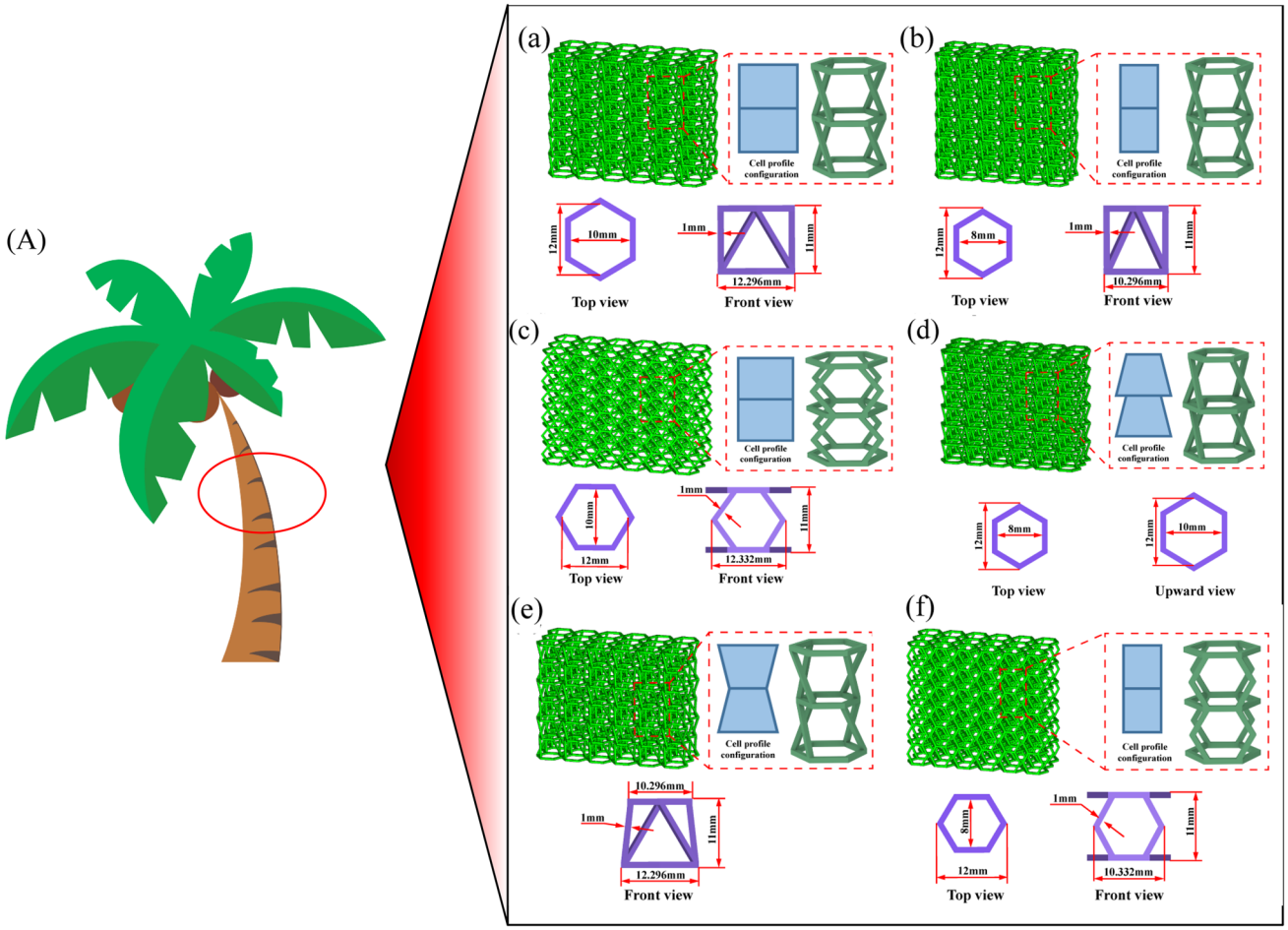

Fig. 1 Bio-inspired structures and feature. **A** A coconut tree with a gradient arrangement of layers and columns. **a** LCHCS. **b** SCHCS. **c** BHS. **d** GHCS. **e** HHCS. **f** SHS. Inspired by the gradient arrangement and columnar arrangement of coconut tree branches, different types of structural design are carried out. Each of the bionic structures is shown in the right magnification of the component cells. Structural dimensions are shown in Fig. 1

Table 1 The mass of six kinds of nylon bionic structures

Structure	BHS	SHS	LCHCS	SCHCS	GHCS	HHCS
Actual mass/g	6.77	5.91	7.17	6.33	9.18	6.75
3D-printed mass/g	6.9	6.00	7.31	6.41	9.31	6.89

Table 2 3D-printing parameters of FS 403P

Parameters	Scanning speed (mm/s)	Build cavity temperature (°C)	Laser power (W)
Tensile sample	7.6	169.5	22
Parameters	Powder layer thickness (mm)	Fill distance (mm)	Material
Tensile sample	0.12	0.15	3300PA

experiment is carried out at a tensile rate of 2 mm/min, as shown in Fig. 2.

In this paper, LS-DYNA is used to analyze bio-inspired structures. The bottom of bio-inspired structures is fully constrained. Bio-inspired structures and the rigid wall are

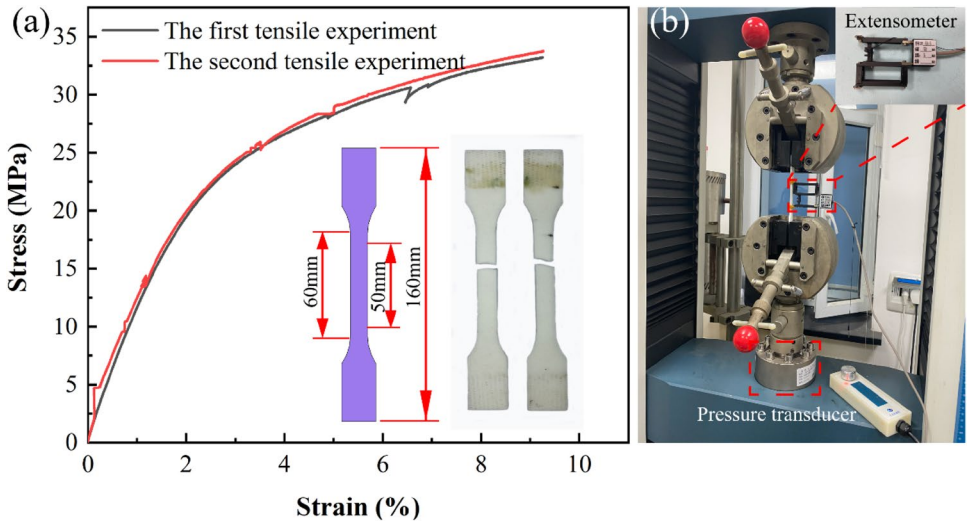

Fig. 2 The material properties of the material test samples. **a** Nylon sample Tensile experimental result. 50 mm is the original gauge length of tensile samples, and 60 mm is the parallel length of tensile samples. **b** Tensile experiment platform

set to #Surface To Surface Contact for avoiding compression penetration between components. The self-contact process is simulated by #Single Surface Contact algorithm. Set up the interface friction factor of 0.2 to better simulate the real process of quasi-static compression [28]. In Cartesian coordinates, the bio-inspired models are divided into three-dimensional tetrahedral elements to simulate the bio-inspired structures. To determine the appropriate size of the structural division grids, the convergence test is conducted. When bio-inspired cells are compressed by 12 mm, the overall absorbed energy of bio-inspired structures that have different size grids is shown in Fig. 3. It can be determined from Fig. 3 that the size of the simulation elements is limited to 0.5 mm.

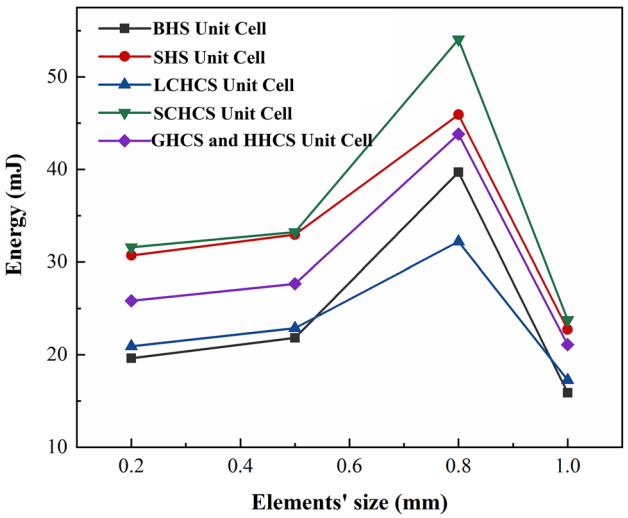

Fig. 3 The convergence test of structures. Since GHCS and HHCS unit cells are identical, a single curve is used to test the convergence of both cells

Similarly, uniaxial compression is performed on the bio-inspired structures under quasi-static loading using the tensile test machine. All experiments are performed at a constant 1.5 mm/min deformation rate. Under the same conditions, experiments are repeated for each chiral honeycomb structure to avoid accidental results.

3 Theoretical Analysis of Quasi-Static Compression

3.1 Analysis of Structures' Compression Characteristics

To verify the mechanical properties of bio-inspired structures, the relative density of bio-inspired structures can be defined as

$$\rho_r = \frac{V_{str}}{V_s}\rho_s, \tag{1}$$

where ρ_r is the absolute density of chiral honeycomb structure. ρ_s is the density of the material. V_{str} is the solid volume of the chiral honeycomb structure. V_s is the space volume of the bio-inspired structure.

According to the geometric relation, the structural volume is

$$V_{honeybeam} = 2t^2 l_k,\ k = e,f, \tag{2}$$

$$V_{beam} = t^2 l_k,\ k = a,b,c,d, \tag{3}$$

$$V_{tsb} = \frac{t^2(l_1 + l_2)}{2}, \tag{4}$$

$$V_{\mathrm{tss}} = \frac{t^2\left(l_3 + l_4\right)}{2}, \tag{5}$$

$$V_{\mathrm{BHS}} = \sum_{n=1}^{n=jk} (2i+1)V_{\mathrm{honeybeam,BHS}} + (k+1)\sum_{N=1}^{N=j}(5i+1)V_{\mathrm{tsb}} - V_{\mathrm{R,BHS}}, \tag{6}$$

$$V_{\mathrm{SHS}} = \sum_{n=1}^{n=jk} (2i+1)V_{\mathrm{honeybeam,SHS}} + (k+1)\sum_{N=1}^{N=j}(5i+1)V_{\mathrm{tss}} - V_{\mathrm{R,SHS}}, \tag{7}$$

$$V_{\mathrm{LCHCS}} = \sum_{n=1}^{n=ijk} 4V_{\mathrm{beam,LCHCS}} + (k+1)\sum_{N=1}^{N=j}(5i+1)V_{\mathrm{tsb}} - V_{\mathrm{R,LCHCS}}, \tag{8}$$

$$V_{\mathrm{SCHCS}} = \sum_{n=1}^{n=ijk} 6V_{\mathrm{beam,SCHCS}} + (k+1)\sum_{N=1}^{N=j}(5i+1)V_{\mathrm{tss}} - V_{\mathrm{R,SCHCS}}, \tag{9}$$

$$V_{\mathrm{GHCS}} = \sum_{n=1}^{n=ijk} 6V_{\mathrm{beam,GHCS}} + (k+1)\sum_{N=1}^{N=j}\left((5i+1)V_{\mathrm{tss}} + (5i+1)V_{\mathrm{tsb}}\right) - V_{\mathrm{R,GHCS}}, \tag{10}$$

$$V_{\mathrm{HHCS}} = \sum_{n=1}^{n=ijk} 6V_{\mathrm{beam,HHCS}} + \frac{k}{2}\sum_{N=1}^{N=ij}(5i+1)V_{\mathrm{tss}} + \left(\frac{k}{2}+1\right)\sum_{N=1}^{N=ij}(5i+1)V_{\mathrm{tsb}} - V_{\mathrm{R,HHCS}}, \tag{11}$$

$$V_{\mathrm{s}} = BTL, \tag{12}$$

where V_{beam} is the volume of a single inclined beam in a bio-inspired structure. $l_{\mathrm{a}}, l_{\mathrm{b}}, l_{\mathrm{c}}, l_{\mathrm{d}}$ are the length of LCHCS, SCHCS, GHCS and HHCS inclined beams, respectively. $l_{\mathrm{e}}, l_{\mathrm{f}}$ are the length of BHS and SHS beams, respectively. l_1, l_2 are the length of the inner and outer sides of the big hexagon, respectively. l_3, l_4 are the length of the inner and outer sides of the small hexagon, respectively. i, j, k are the number of the bio-inspired structural cells in the direction of Cartesian coordinate system. V_{tsb}, V_{tss} are one-sixth of the three-dimensional large and small hexagonal volume of the structural top. V_{R} is the overlapped volume of bio-inspired structures. The overlap is quadratic and is ignored in the calculation. V_{s} is the space volume occupied by bio-inspired structures. B, T, L are the thickness, width and height of the space volume occupied by bio-inspired structures.

Due to the complexity of bio-inspired structures, the solid volume of the bio-inspired structures can be directly obtained by calculating the truss beam. The relative density of bio-inspired structures are

$$\frac{\rho_{\mathrm{BHS}}}{\rho_{\mathrm{s}}} = \frac{V_{\mathrm{BHS}}}{V_{\mathrm{s,BHS}}} = 0.0429, \tag{13}$$

$$\frac{\rho_{\mathrm{SHS}}}{\rho_{\mathrm{s}}} = \frac{V_{\mathrm{SHS}}}{V_{\mathrm{s,SHS}}} = 0.0593, \tag{14}$$

$$\frac{\rho_{\mathrm{LCHCS}}}{\rho_{\mathrm{s}}} = \frac{V_{\mathrm{LCHCS}}}{V_{\mathrm{s,LCHCS}}} = 0.0526, \tag{15}$$

$$\frac{\rho_{\mathrm{SCHCS}}}{\rho_{\mathrm{s}}} = \frac{V_{\mathrm{SCHCS}}}{V_{\mathrm{s,SCHCS}}} = 0.0683, \tag{16}$$

$$\frac{\rho_{\mathrm{GHCS}}}{\rho_{\mathrm{s}}} = \frac{V_{\mathrm{GHCS}}}{V_{\mathrm{s,GHCS}}} = 0.0972, \tag{17}$$

$$\frac{\rho_{\mathrm{HHCS}}}{\rho_{\mathrm{s}}} = \frac{V_{\mathrm{HHCS}}}{V_{\mathrm{s,HHCS}}} = 0.0495, \tag{18}$$

The three-dimension bio-inspired structures belong to new superstructures and the compression process is complex. The error of the traditional theory of mechanical equilibrium is large. Therefore, this paper starts from the perspective of functional principle [27]. It is obtained using Hamilton's principle.

$$\delta J = \delta\int_{\mathrm{t_0}}^{\mathrm{t_1}} L\mathrm{d}t - \delta\int_{\mathrm{t_0}}^{\mathrm{t_1}} D\mathrm{d}t = 0. \tag{19}$$

During quasi-static compression, the structural velocity V=0. The kinetic energy of the compressed bio-inspired structures is ignored and the functional relationship transformation occurs. In the quasi-static compression process, the compression transient energy is

$$\begin{aligned}\mathrm{d}W &= \iint_S F_y \mathrm{d}u\mathrm{d}S + \iiint_V B\mathrm{d}\mathbf{u}\mathrm{d}V = \iiint_V \sigma_{ij}\mathrm{d}\left(\frac{\partial u_i}{\partial x_j}\right)\mathrm{d}V \\ &= \iiint_V \sigma_{ij}\mathrm{d}\left[\frac{1}{2}\left(\frac{\partial u_i}{\partial x_j} + \frac{\partial u_j}{\partial x_i}\right)\right]\mathrm{d}V = \iiint_V \sigma_{ij}\mathrm{d}\varepsilon_{ij}\mathrm{d}V = \overline{\sigma}S\Delta H.\end{aligned} \tag{20}$$

Structural energy consumption is equivalent to the energy consumption of plastic hinge at the corner of the bio-inspired structures. There are two kinds of plastic hinge energy consumption, namely structural bending energy consumption and structural torsion energy consumption.

$$E = n_1 M_1 \Delta\theta + n_2 M_2 \Delta\varphi, \tag{21}$$

where E is the energy dissipation of structural bending plastic hinge and torsion plastic hinge. M_1 is the structural bending moment M_2 is structural torque. n_1 and n_2 is number of hinges with bending and torsion energy dissipation.

Therefore, the compression load of bio-inspired structures in the large deformation stage (compression platform period) is

$$\overline{F}_{\mathrm{BHS}} = \frac{n_1 \sigma_{\mathrm{ys}} t^3 \Delta\theta_1}{\Delta H_1}, \tag{22}$$

$$\overline{F}_{\mathrm{SHS}} = \frac{n_2 \sigma_{\mathrm{ys}} t^3 \Delta\theta_2}{\Delta H_2}, \tag{23}$$

$$\overline{F}_{\mathrm{LCHCS}} = \frac{n_3 \sigma_{\mathrm{ys}} t^3 \Delta\theta_3}{\Delta H_3} + \frac{n_3 \sigma_{\mathrm{ys}} t^3 \Delta\varphi_3}{\Delta H_3}, \tag{24}$$

$$\overline{F}_{\mathrm{SCHCS}} = \frac{n_4 \sigma_{\mathrm{ys}} t^3 \Delta\theta_4}{\Delta H_4} + \frac{n_4 \sigma_{\mathrm{ys}} t^3 \Delta\varphi_4}{\Delta H_4}, \tag{25}$$

$$\overline{F}_{\mathrm{GHCS}} = \frac{n_5 \sigma_{\mathrm{ys}} t^3 \Delta\theta_5}{\Delta H_5} + \frac{n_5 \sigma_{\mathrm{ys}} t^3 \Delta\varphi_5}{\Delta H_5}, \tag{26}$$

$$\overline{F}_{\mathrm{HHCS}} = \frac{n_6 \sigma_{\mathrm{ys}} t^3 \Delta\theta_6}{\Delta H_6} + \frac{n_6 \sigma_{\mathrm{ys}} t^3 \Delta\varphi_6}{\Delta H_6}, \tag{27}$$

where $n_1 = n_2 = 2 \times 4 \times 6 \times 6 = 288$, $n_3 = n_4 = n_5 = n_6 = 4 \times 3 \times 6 \times 6 = 432$. $\Delta H_i (i = 1, 2, 3, 4, 5, 6)$ is press displacement, $\Delta h \geq 6$ mm. $\Delta\theta$ is curving angle of bio-inspired structures' beams, $\Delta\theta_1 = \Delta\theta_2 = \frac{\pi \arcsin(h/2L)}{180} - \frac{\pi \arcsin(h/2L - \Delta H/12L)}{180}$, $h_{\mathrm{BHS}} = h_{\mathrm{SHS}} = 4.5\mathrm{mm}$, $h_{\mathrm{LCHCS}} = h_{\mathrm{SCHCS}} = h_{\mathrm{GHCS}} = h_{\mathrm{HHCS}} = 9\mathrm{mm}$, $L_{\mathrm{BHS}} = 5.868\mathrm{mm}$, $L_{\mathrm{SHS}} = 5.197\mathrm{mm}$, $L_{\mathrm{LCHCS}} = 10.711\mathrm{mm}$, $L_{\mathrm{SCHCS}} = 10.155\mathrm{mm}$, $L_{\mathrm{GHCS}} = L_{\mathrm{HHCS}} = 10.559\mathrm{mm}$, $\Delta\theta_3 = \Delta\theta_4 = \Delta\theta_5 = \Delta\theta_6 = \frac{\pi \arcsin(h/L)}{180} - \frac{\pi \arcsin(h/L - \Delta H/6L)}{180}$. $\Delta\varphi_i (i = 3, 4, 5, 6)$ is the torsional angle of chiral structures, $\Delta\varphi_i = \frac{\pi \arctan(0.1\Delta H/L)}{180}$.

The structural compression force is divided into three stages: elastic section, yield section, and dense section. Gibson et al. [29] obtained by integrating the constitutive model of structural compression.

$$\sigma = \begin{cases} E\varepsilon, \ \sigma \leq \sigma_{\mathrm{y}} \\ \sigma_{\mathrm{y}}, \ \varepsilon_{\mathrm{y}} \leq \varepsilon \leq \varepsilon_{\mathrm{D}}\left(1 - D^{-1}\right) + \varepsilon_{\mathrm{y}} \\ \sigma_{\mathrm{y}} \dfrac{1}{D} \left(\dfrac{\varepsilon_{\mathrm{D}}}{\varepsilon_{\mathrm{D}} - \varepsilon} \right)^{\mathrm{m}}, \ \varepsilon > \varepsilon_{\mathrm{D}}\left(1 - D^{-1}\right) + \varepsilon_{\mathrm{y}}, \end{cases} \tag{28}$$

where σ is structural stress. ε is structural strain. E is elastic modulus. σ_{y} is structural yield stress. ε_{y} is structural yield strain. ε_{D} is the strain when the structure is dense. D and m are constant.

To simplify the compressive mechanical relationship of structures and better describe the stress–strain relationship, Rush model [30] was proposed

$$\sigma = A\varepsilon^m + B\varepsilon^n, \ \ 0 < m < 1 \ \text{and} \ 1 < n < \infty. \tag{29}$$

Although the proposed model simplifies the whole compression constitutive model, its accuracy in describing the compaction stage is insufficient.

To more accurately build the multi-stage load of bio-inspired structures, the constitutive models [31] of the bio-inspired structures are established by model hypothesis and parameter fitting based on the compression response of the quasi-static compression experiments. The continuous function method is used to construct the constitutive relationship for improving the accuracy of the results.

$$F = a_1 \mathrm{e}^{-a_2 x} \sin\left(a_3 x\right) + a_4 \tanh\left(a_5 x\right) + a_6 \tan\left(a_7 x\right), \tag{30}$$

where F is the compression load of bio-inspired structure. a_1, a_2, a_3, a_4, a_5, a_6, a_7 are the simulators and parameters. x is the compression displacement. In the fitting relation of constitutive equation, the product of exponential function and sinusoidal function in the first item is the elastic period and yield period of compression. The hyperbolic tangent function in the second item is the plateau period in the compression process. The tangent function in the third term is the compact period of compression. The trinomial interaction is used to accurately express the force–displacement relations at each stage of the compression process of chiral structures.

Based on the force–displacement data obtained from the compression experiments, the improved global simulated annealing (SA) algorithm [32] is used to identify the parameters and the specific process is shown in Fig. 4. The iteration repetition number is 400, and the control iteration number is 300. The obtained data results are as shown in Table 3.

In Table 3, R represents fitting correlation.

$$R = \frac{\mathrm{Cov}(x, F)}{\sqrt{\mathrm{Var}[x]\mathrm{Var}[F]}}, \tag{31}$$

where Cov (x, F) is the covariance of x and F. Var$[x]$ and Var$[F]$ is the variance of x and F, respectively.

The accuracy of the parametric results can be seen from the result in Fig. 5. The structural constitutive equations can basically represent the compression process of the

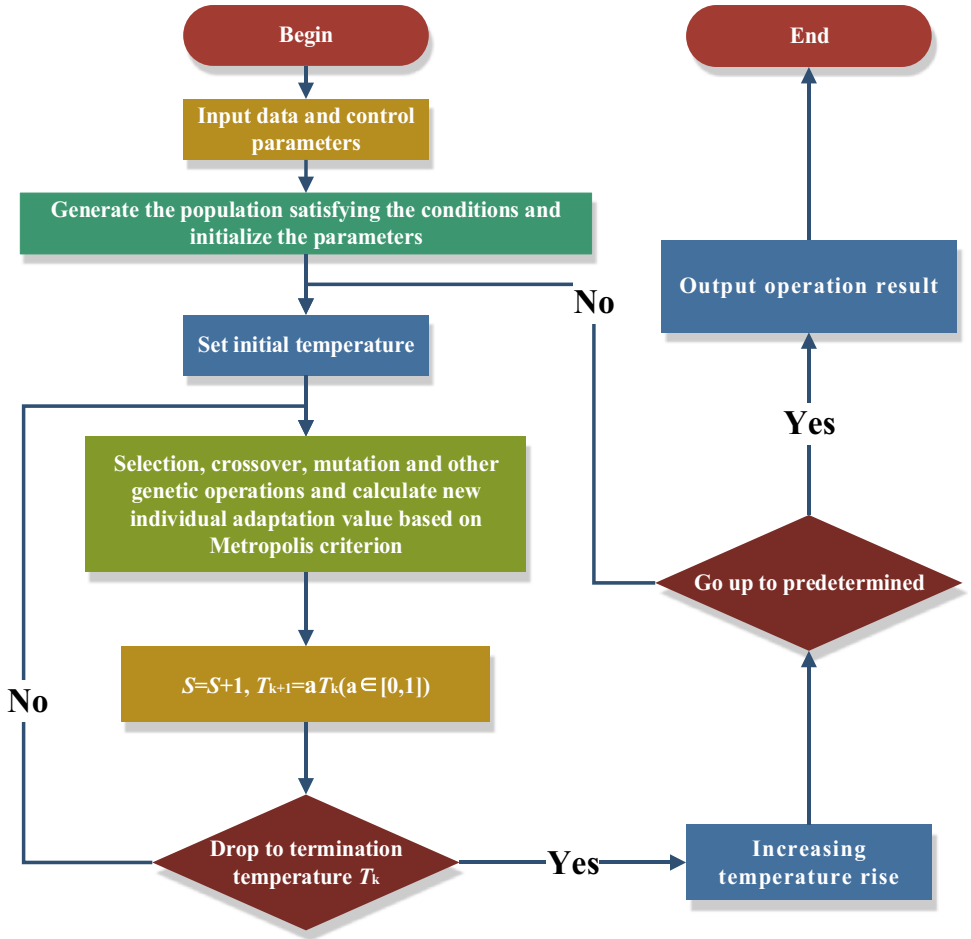

Fig. 4 The improved global simulated annealing (SA) algorithm process. In the algorithm, the temperature is the parameter set, and the initial temperature is the initial parameter set

Table 3 Structural constitutive relation results

	a_1	a_2	a_3	a_4	a_5	a_6	a_7	R
BHS	−114.8	0.1	0.1	75.2	0.5	43.4	−0.04	0.98
SHS	41.8	0.4	0.5	40.0	0.6	−61	0.01	0.98
LCHCS	−1095.6	0.2	0.1	280.2	1.0	−351.2	0.03	0.97
SCHCS	−250.2	0.6	−0.8	−79.2	−1.0	22.5	0.07	0.85
GHCS	919.0	0.2	−0.1	251.2	1.2	540.5	−0.01	0.86
HHCS	613.4	0.1	−0.1	186.8	1.0	127.3	−0.03	0.97

chiral honeycomb structures, and the fitting degree error is within 15%.

3.2 Structural Protection Criterion

To accurately and quantitatively measure protective performance of the bio-inspired structure, some necessary evaluation indicators are used [33].

Internal energy absorption EA of structural deformation is calculated, as shown in Eq. (32)

$$\mathrm{EA} = \int_0^{x_0} F\mathrm{d}x, \tag{32}$$

where x_0 is the quasi-static compression displacement, F is quasi-static payload during compression.

SEA1 and SEA2 are important indicators of energy absorption unit mass and unit volume, as showed in Eqs. (33) and (34).

$$\mathrm{SEA1} = \frac{\mathrm{EA}}{M}, \tag{33}$$

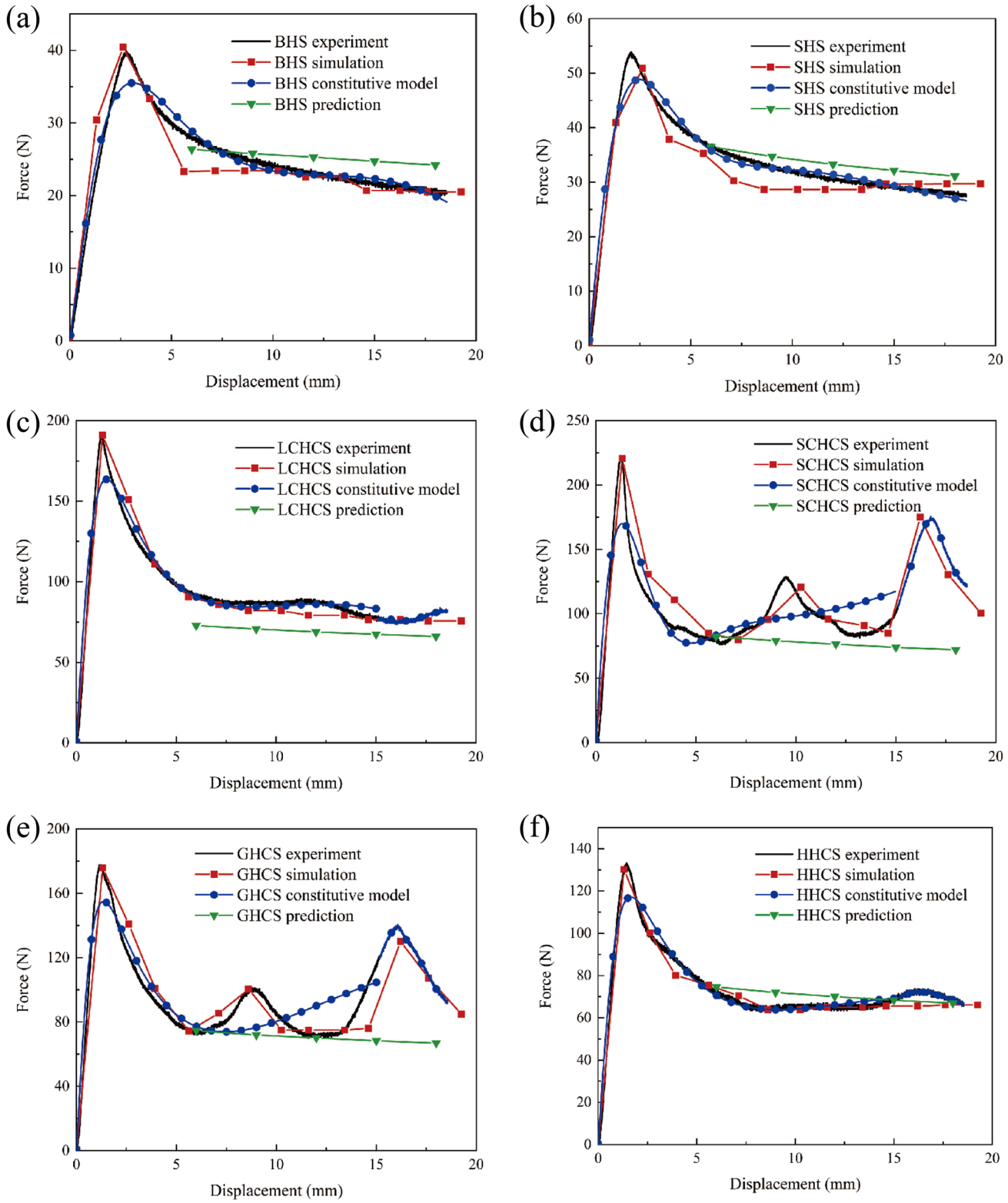

Fig. 5 Force–displacement curves theoretically, experimentally and numerically of the bio-inspired structures. **a** BHS force–displacement curve. **b** SHS force–displacement curve. **c** LCHCS force–displacement curve. **d** SCHCS force–displacement curve. **e** GHCS force–displacement curve. **f** HHCS force–displacement curve

$$\mathrm{SEA2} = \frac{\mathrm{EA}}{V}, \tag{34}$$

where M is the structural mass and V is the structural volume. Given the importance of SEA in protective design, High SEA are extremely critical within applications of protective engineering.

PF is the maximum force during compression and it is calculated as Eq. (35):

$$\mathrm{PF} = \max\left(F(x)\right). \tag{35}$$

SS is the specific strength during the compression of the structure, as shown in Eq. (36):

$$\mathrm{SS} = \frac{\sigma_{\max}}{\rho_{\mathrm{str}}}, \tag{36}$$

where ρ_{str} is density of the whole bio-inspired structure. The bigger SS, the better the structural performance. It is a main index to measure the light weight and high strength of structures.

4 Compression Properties of Bio-inspired Structures

In this paper, the corresponding force–displacement curves of the bio-inspired structures under the condition of quasi-static axial compression are studied, as shown in Fig. 5.

It can be seen from Fig. 5a–f that as the displacement increases, the force increases linearly in the initial stage of compression, i.e., the elastic period of compression. However, local damage occurs inside the structures after the structural strain reaches yield and the transfer route of structural force is offset. The structural compression load decreases to some extent. When the load is reduced to a certain extent, the bio-inspired structure is in the overall yield section, and the load is basically unchanged. Due to the low compression speed in the quasi-static compression process, the structural energy is mainly stored as internal energy. After the external load work is converted into structural energy, the bio-inspired structure dissipates internal energy through plastic hinge energy dissipation, that is, the yield stage of the structure is the main energy absorption stage. As shown in Fig. 5, the maximum compression loads of the bio-inspired structures are 39.4N, 53.9N, 190.8N, 221.4N, 177.7N and 133.3N, respectively. SCHCS has the highest bearing capacity, followed by LCHCS. The bearing capacity of SCHCS is 561.9%, 410.8% 116.0%, 124.6% and 166.1% of BHS, SHS, LCHCS, GHCS and HHCS. It can be seen from Fig. 5 that the curve of prediction model is consistent with the trend of experimental curve. The coincidence degree between the predicted model results and experimental results is up to 85%. Compared with the experimental results, the coincidence degree of mechanical model is more than 85%, which can predict the experimental load well as shown in Table 4. At the same time, the influence of SEA and CFE parameters is considered. The mechanical properties of the bio-inspired structures are shown in Fig. 6.

It can be seen from Fig. 6a–f that the overall comprehensive characteristics of the bionic structure, ECHS is the best, that is, LCHCS and SCHCS have the best mechanical properties. The *SS* of SCHCS is 515.1%, 357.8%, 214.3%, 240.1% and 177.5% of the other bio-inspired structures. Meanwhile, the SEA1, SEA2 and EA of SCHCS are also the highest, whose SEA1 is 468.2%, 302.8%, 129.8%, 161.4%, 156.7% of others and SEA2 is 644.4%, 324.4%, 168.9%, 163.7%, 216.0% of others and EA is 438.1%, 324.4%, 114.8%, 111.3%, 146.8% of others, indicating that SCHCS has the best mechanical properties. However, LCHCS shows stable force and great failure stability. At the same time, the SS, SEA and EA are great. The mechanical properties of the chiral honeycomb structures with equal width like bamboo joints are excellent, which are superior to other bio-inspired structures. The structural compression properties of polymer materials in existing papers [34–36]are compared, as shown in Fig. 7.

It can be seen from Fig. 7 that designed chiral honeycomb structures have good energy absorption properties. During the compression process of bio-inspired structures, the plastic hinge characteristics among the trusses lead to stress concentration phenomenon, which leads to structural damage. To compare the protection performance of BHS, SHS, LCHCS, SCHCS, GHCS and HHCS, the stress nephograms and the deformation modes during the quasi-static compression process, as shown in Fig. 8.

It can be seen from Fig. 8 that the stress concentration degree of the bio-inspired structures is slightly different in

Table 4 The error of the mechanical model and structural constitutive model

Structure	BHS	SHS	LCHCS	SCHCS	GHCS	HHCS
The error of the mechanical model /%	93	91	88	85	85	92
The error of structural constitutive model /%	98	98	97	85	86	97

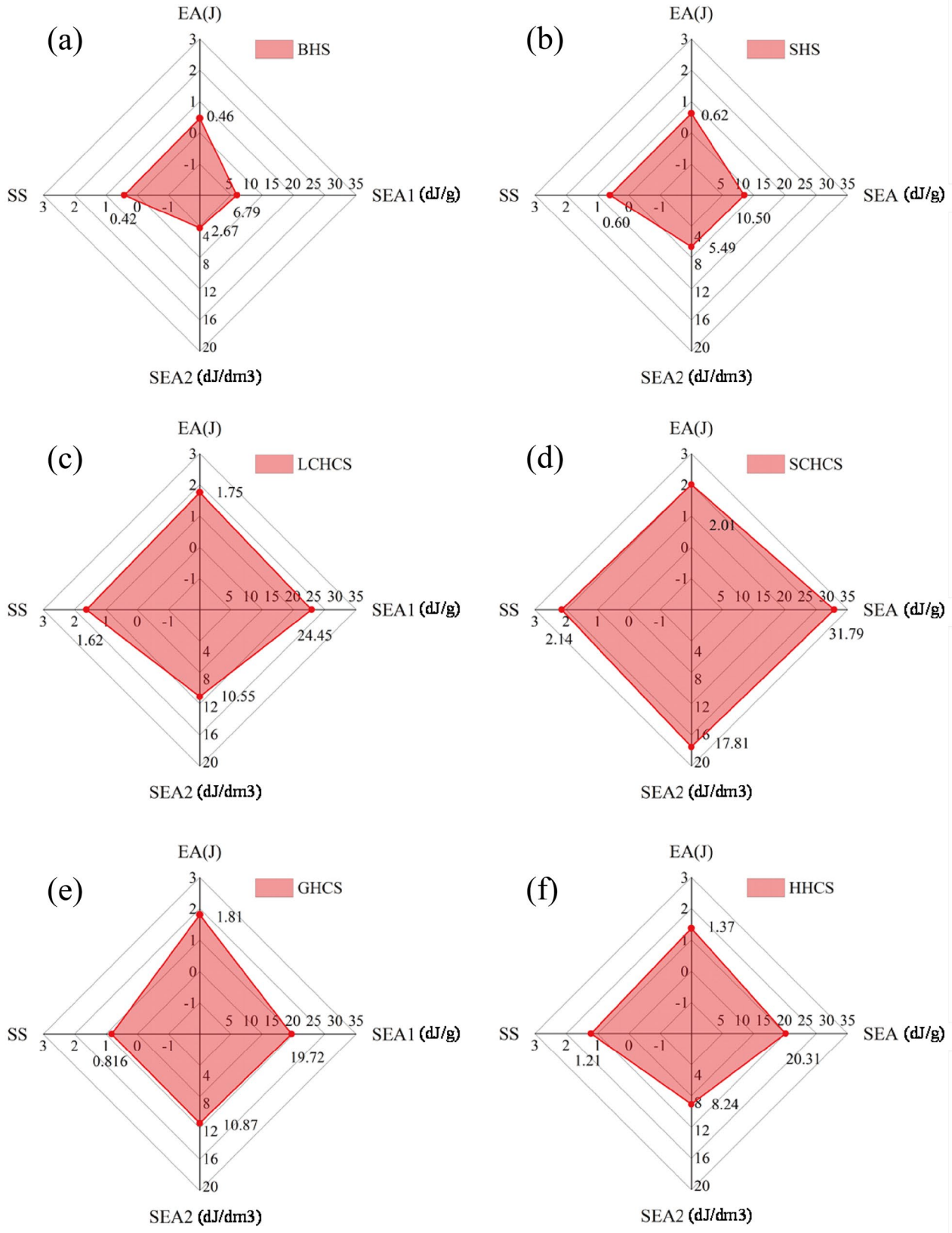

Fig. 6 Mechanical characteristics of the bio-inspired structures. **a** BHS properties radar figure. **b** SHS properties radar figure. **c** LCHCS properties radar figure. **d** SCHCS properties radar figure. **e** GHCS properties radar figure. **f** HHCS properties radar figure

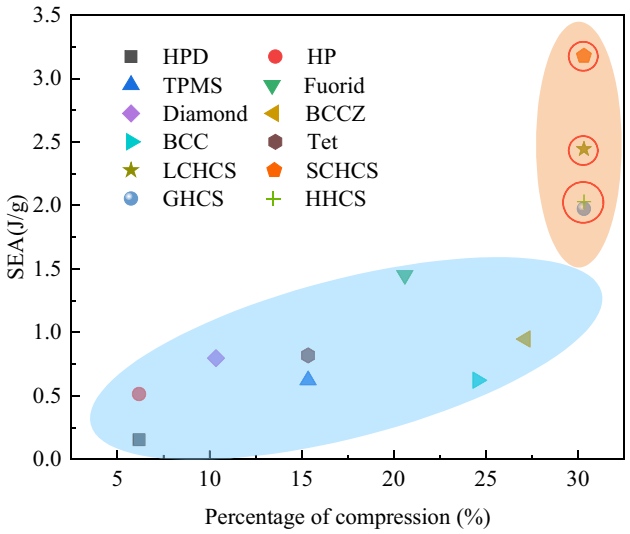

Fig. 7 Comparison of structural SEA. The points circled in red are four chiral honeycomb structures in this paper

the process of uniaxial compression. Under the same displacement, i.e. the same axial strain, LCHCS and HHCS have uniform distribution of stress. All bio-inspired chiral structures are in the form of one-line compression and honeycomb structures are multi-bending deformation and X-shaped multilayer deformation in the compression process. The existence of the one-line deformation modes improves the energy absorption rate of the bio-inspired structures (Fig. 8). The compression process of the three shapes in two directions in the plane all presents a progressive buckling deformation mode. At the beginning of the collapse process, the chiral honeycomb structures collapse into a horizontal deformation band at the middle end, and then gradually collapse from both ends, and finally reach obvious compaction state. The deformation is more stable on the whole and the existence of this phenomenon leads to a small carrying capacity. By comparing EA, SEA1, SEA2 and SS of bio-inspired structures of different sizes, it can be seen that the performance of SCHCS is better than that of the other three bio-inspired structures at the same compressive strain rate. Thus, it is of great application and research value to carry out different structural transformation of the same type of energy-absorbing structure. When manufacturing protective applications, keeping the equiaxed chiral honeycomb structure (Similar to bamboo) makes the structure have better protection characteristics.

To further explore the influence of structural sizes, the mechanical properties of the bio-inspired structures with the size of the hexagon reduced are compared. The bearing capacity and energy absorption of ECHS, GHCS and HHCS at different sizes are shown in Fig. 9.

In this study, the size of the honeycomb cell is taken as the variable x, and EA and bearing capacity F are taken as the objectives. When the size of cell is reduced to 4 mm, EA of ECHS, GHCS, and HHCS basically reaches the maximum value, but the maximal bearing capacity F still increases with the size decreasing. The mechanical properties of bio-inspired structures largely depend on the selection of size. The selection of small size is very important in the optimal design of bio-inspired structures. While the structural requirements are changed to carrying capacity and load stability, the size of structural units should be appropriately expanded within the range of load capacity. When the carrying capacity is required, the structural unit

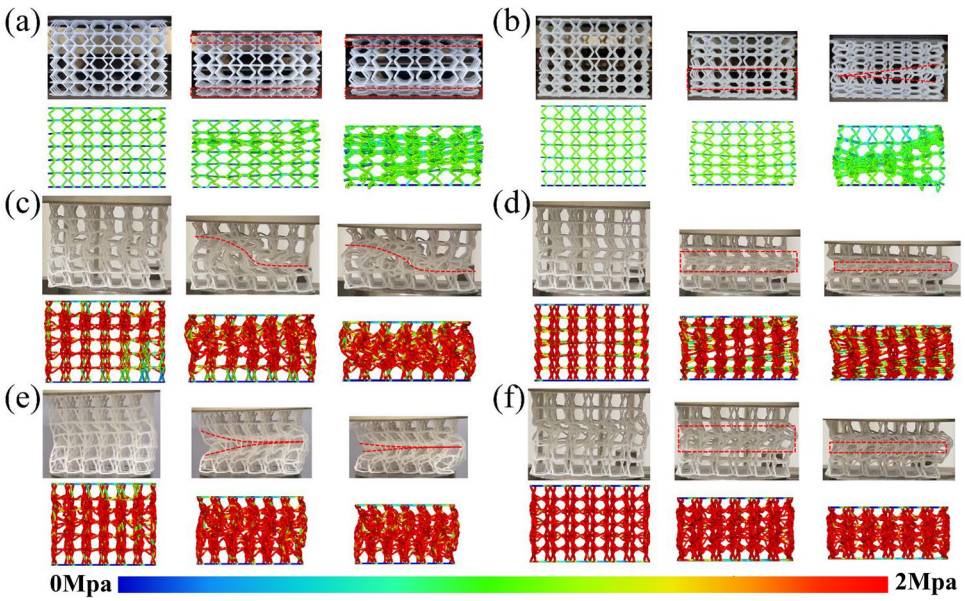

Fig. 8 The deformation process of bio-inspired structures at various stages of compression. **a** The deformation process of BHS. **b** The deformation process of SHS. **c** The deformation process of LCHCS. **d** The deformation process of GHCS. **e** The deformation process of SCHCS. **f** The deformation process of HHCS

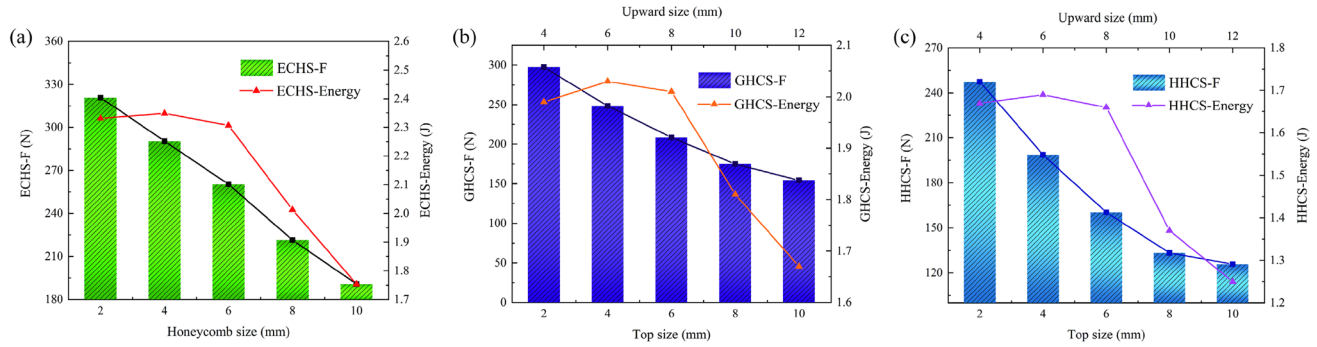

Fig. 9 F and EA of ECHS, GHCS and HHCS at different sizes. **a** Dimensional variation performance of ECHS. **b** Dimensional variation performance of GHCS. **c** Dimensional variation performance of HHCS

can be appropriately reduced or multi-level structure can be carried out (multi-level structure design). Therefore, in the next step, we will carry out multi-level optimization design and mechanical characteristics analysis of the bio-inspired structures.

5 Conclusions

In this paper, four types of chiral honeycomb structures inspired by the biological arrangement shape are manufactured by 3D printing. The functional principle is proposed to solve the large deformation response and the structural constitutive relations are used to explain the structural mechanical properties. Compared with the experimental results, the mechanical models based on the functional theory and constitutive relation is accurate, and the errors are all within 15%. ECHS has the best mechanical properties, among which SCHCS has the best performance. SCHCS has the most excellent *F*, SEA, EA and SS performance. The numerical model verifies that the bearing capacity of ECHS, GHCS, and HHCS increases with the decrease of the sizes. The energy absorption of bionic structures increases first and then remains unchanged with the decrease of size.

Acknowledgements This work is supported by National Key R&D program of of China (No. 2022YFB4600500), the National Natural Science Foundation of China (No. 51975246), the Science and Technology Development Program of Jilin Province, China (No. 20220101192JC), Capital construction fund plan within the budget of Jilin Province (No. 2023C041-4), Chongqing Natural Science Foundation (No. CSSTB2022NSCQ-MSX0225).

Author contributions RL: writing—original draft, writing—review and editing, visualization, project administration, data curation, formal analysis, methodology, software, formal analysis. GY: writing—review and editing, visualization, supervision, conceptualization, validation. ZX: writing—review and editing. XG: writing—review and editing. KG: writing—review and editing. JL: writing—review and editing. ZY: writing—review and editing, visualization, funding acquisition, resources, conceptualization, validation. PL: writing—review and editing, visualization, funding acquisition. ZZ: writing—review and editing. CH: writing—review and editing.

Data Availability The data that support the findings of this study are not openly available due to some restrictions and are available from the corresponding author upon reasonable request.

Declarations

Conflict of interest On behalf of all authors, the corresponding author states that there is no conflict of interest.

References

1. Pana-Cryan, R., & Myers, M. L. (2010). Effectiveness of roll-over protective structures in reducing farm tractor fatalities. *American Journal of Preventive Medicine, 42*, 68–71.
2. Yun, X., & Yang, J. L. (2021). A design strategy of bio-inspired defensive structures with stiffness programmability for reusable impact-resistance protection. *International Journal of Impact Engineering, 157*, 103982.
3. Yang, X. F., Ma, J. X., Shi, Y. L., Sun, Y. X., & Yang, J. L. (2017). Crashworthiness investigation of the bio-inspired bi-directionally corrugated core sandwich panel under quasi-static crushing load. *Materials & Design, 135*, 275–290.
4. Larmet, Y., Reibel, S., Carnahan, J., Nawa, H., Marescaux, C., & Depaulis, A. (1995). Protective effects of brain-derived neurotrophic factor on the development of hippocampal kindling in the rat. *NeuroReport, 6*, 1937–1941.
5. Lathrop, B., & Sennett, R. (1968). Effects of hypervelocity impact on honeycomb structures. *Journal of Spacecraft and Rockets, 5*, 1496–1497.
6. Richardson, S., Rechnitzer, G., Orton, T., Shifman, M., Crocker, S., Ramharuk, A., Jones, C., & Indurjit, P. (2009). Development of rollover protective structures for mining light vehicles. *Sae Technical Papers, 2015*, 1–17.
7. Dumont, A., Grosse, B., & Slater, C. (2009). Requirements for comparing the performance of finite element models of biological structures. *Journal of Theoretical Biology, 256*, 96–103.

8. Gargano, A., Pingkarawat, K., Blacklock, M., Pickerd, V., & Mouritz, A. (2017). Comparative assessment of the explosive blast performance of carbon and glass fibre-polymer composites used in naval ship structures. *Composite Structures, 171*, 306–316.
9. Hu, L., Etza, B., & Bing, F. (2021). In-plane dynamic crushing of a novel honeycomb with functionally graded fractal self-similarity. *Composite Structures, 270*, 114106.
10. Alderson, A., Alderson, K., Attard, D., Evans, K., Gatt, R., Grima, J., Miller, W., Ravirala, N., Smith, C., & Zied, K. (2010). Elastic constants of 3-, 4- and 6-connected chiral and anti-chiral honeycombs subject to uniaxial in-plane loading. *Composites Science & Technology, 70*, 1042–1048.
11. Frenzel, T., Kadic, M., & Wegener, M. (2017). Three-dimensional mechanical metamaterials with a twist. *Science, 358*, 1072–1074.
12. Lin, G., Li, G. J., Chen, P., Sun, P. W., Chizhik, W. F., Makhaniok, A. S., Melnikova, A. A., Kuznetsova, G. B., & Tatiana, A. (2021). Buckling of lattice columns made from three-dimensional chiral mechanical metamaterials. *International Journal of Mechanical Sciences, 194*, 106208.
13. Zhong, R. C., Fu, M. H., Chen, X., Zheng, B. B., & Hu, L. L. (2019). A novel three-dimensional mechanical metamaterial with compression-torsion properties. *Composite Structures, 226*, 111232.
14. Shafighfard, T., Cender, T., & Demir, E. (2020). Additive manufacturing of compliance optimized variable stiffness composites through short fiber alignment along curvilinear paths. *Additive Manufacturing, 37*, 101728.
15. Li, D., Yin, J., Dong, L., & Roderic, S. (2018). Strong re-entrant cellular structures with negative Poisson's ratio. *Springer, US, 53*, 3493–3499.
16. Restrepo, D., Mankame, N. D., & Zavattieri, P. D. (2015). Phase transforming cellular materials. *Extreme Mechanics Letters, 4*, 52–60.
17. Ajdari, A., Hamid, N., & Ashkan, V. (2010). Dynamic crushing and energy absorption of regular, irregular and functionally graded cellular structures. *International Journal of Solids and Structures, 48*, 506–516.
18. Liu, R. Y., Yao, G. F., Xu, Z. Z., Guo, X., Gao, K. Y., Cao, Q., Yu, Z. L., Zhang, Z. H., Han, C. Y., & Liu, J. B. (2022). Study on functional mechanical performance of honeycomb array structures inspired by gideon beetle. *Journal of Bionic Engineering, 19*, 1024–1035.
19. Peng, X., Zhang, B., Wang, Z., Su, W., Niu, S., Han, Z., & Ren, L. (2022). Bio-inspired strategies for excellent mechanical properties of composites. *Journal of Bionic Engineering, 19*, 1203–1228.
20. Song, K. D., Zhang, D. M., Yin, J., & Huang, Y. (2021). Computational study of extrusion bioprinting with Jammed Gelatin microgel-based composite ink. *Additive Manufacturing, 41*, 101963.
21. Ibrahim, H., Jahadakbar, A., Dehghan, A., Moghaddam, N., Amerinatanzi, A., & Elahinia, M. (2018). In vitro corrosion assessment of additively manufactured porous NiTi structures for bone fixation applications. *Metals, 8*, 164.
22. Chang, Q., Feng, J., Chen, Y., & Shu, Y. (2019). In-plane crushing response of tetra-chiral honeycombs. *International Journal of Impact Engineering, 130*, 247–265.
23. Zhang, X., Xie, J., Chen, J. X., Okabe, Y., Pan, L., & Xu, M. (2017). The beetle elytron plate: A lightweight, high-strength and buffering functional-structural bionic material. *Scientific Reports, 7*, 4440.
24. Plessis, A., Broeckhoven, C., Yadroitsev, I., Yadroitsava, I., & Roux, S. (2018). Analyzing nature's protective design: The glyptodont body armor. *Journal of the Mechanical Behavior of Biomedical Materials, 82*, 218–223.
25. Wang, D., Yang, Y. Q., Liu, R. C., Xiao, D. M., & Sun, J. F. (2013). Study on the designing rules and processability of porous structure based on selective laser melting (SLM). *Journal of Materials Processing Technology, 213*, 1734–1742.
26. Gu, D., Meiners, W., Wissenbach, K., & Poprawe, R. (2012). Laser additive manufacturing of metallic components: Materials, processes and mechanisms. *International Materials Reviews, 57*, 133–164.
27. Xiao, L. J., & Song, W. D. (2018). Additively-manufactured functionally graded Ti-6Al-4V lattice structures with high strength under static and dynamic loading: Experiments. *International Journal of Impact Engineering, 111*, 255–272.
28. Yao, G. F., Liu, R. Y., Xu, Z. Z., Xin, R. L., Chen, L. X., Yu, Z. L., & Zhang, Z. H. (2021). Study on quasi-static mechanical properties of four 3D-printed bio-inspired structures based on functional relationship. *Composite Structures, 274*, 114304.
29. Gibson, L., & Ashby, M. (1997). *Cellular solids: Structure and properties* (pp. 187–201). Cambridge University Press.
30. Avalle, M., Belingardi, G., & Ibba, A. (2007). Mechanical models of cellular solids: Parameters identification from experimental tests. *International Journal of Impact Engineering, 34*, 3–27.
31. Mohr, D., Xiao, Z. Y., & Vaziri, A. (2006). Quasi-static punch indentation of a honeycomb sandwich plate: Experiments and modelling. *Journal of Mechanics of Materials & Structures, 1*, 581–604.
32. Zhu, J. N., Borisov, E., Liang, X. H., Farber, E., Hermans, M. J. M., & Popovich, V. A. (2020). Predictive analytical modelling and experimental validation of processing maps in additive manufacturing of nitinol alloys. *Additive Manufacturing, 38*, 101802.
33. Liang, M., Shi, J. X., Yang, C., & Gao, T. (2020). An emerging class of hyperbolic lattice exhibiting tunable elastic properties and impact absorption through chiral twisting. *Extreme Mechanics Letters, 40*, 100869.
34. Korshunova, N., Alaimo, G., Hosseini, S. B., Carraturo, M., Reali, A., Niiranen, J., Auricchio, F., Rank, E., & Kollmannsberger, S. (2021). Bending behavior of octet-truss lattice structures: Modelling options, numerical characterization and experimental validation. *Materials & Design, 205*, 109693.
35. Hu, Y., Fang, Q. Z., & Qian, J. (2021). Effect of cell structure on the uniaxial compression properties of closed-cell foam materials. *Materials Today Communications, 26*, 102104.
36. Tian, Z. Y., Yan, Y., Li, J., Hong, Y., & Guo, F. L. (2017). Progressive damage and failure analysis of three-dimensional braided composites subjected to biaxial tension and compression. *Composite Structures, 185*, 496–507.